Commun. Comput. Phys.
doi: 10.4208/cicp.OA-2024-0295

Vol. **39**, No. 5, pp. 1454-1478
May 2026

Gas-Kinetic Unified Algorithm for Multi-Component Monatomic Gas Mixture

Fan Li[1] and Zhi-Hui Li[1,*]

[1] *China Aerodynamics Research and Development Center, Mianyang 621000, China.*

Received 6 December 2024; Accepted (in revised version) 25 April 2025

Abstract. In recent decades, gas-kinetic unified algorithm (GKUA) based on Boltzmann model equation has been proposed, which is suitable for the whole regimes gas flows. The original GKUA is designed for single-component gas flows. In this work, we extend GKUA to multi-component monatomic gas mixture flows based on the Andries-Aoki-Perthame (AAP) model. The algorithm are validated by the steady normal shock wave structure problem, the flow around two-dimensional circular cylinder and the pressure/temperature gradient driven microchannel flow problems. Simulation results are in good agreement with those obtained by other methods, which verifies the reliability of the proposed algorithm for the simulation of multi-component monatomic gas mixture. Then, taking the 25N attitude control engine two-dimensional profile as the object, the study of two-dimensional profile nozzle internal and external mixed flow problem is carried out, and the influences of the component concentration ratio and mass ratio on the molecular transport in the engine internal and external mixed flow field are discussed.

AMS subject classifications: 35Q20, 76P05, 82C40

Key words: Gas mixture, gas-kinetic unified algorithm, Boltzmann model equation, vacuum plume, microchannel flow.

1 Introduction

Vacuum plume problem of attitude orbit control engine of in-orbit spacecraft is a cross-regime problem involving continuum flow, rarefied transition flow and free molecular flow. Engine gas is a multi-component gas mixture. In addition to the common characteristics of the general single-component gas flow, the gas flow also involves the interaction between components and between components and solid boundary, producing phenomena such as Baro diffusion and Ghost effect [1,2], and the transport mechanism is

*Corresponding author. *Email addresses:* 748867007@qq.com (F. Li), lizhihui@cardc.cn (Z.-H. Li)

complex. Multi-component gas mixture flow involves pressure gradient driven, temperature gradient driven and concentration gradient driven. The diffusion and flow of the gas will drive the mass transport and affect the flow [3,4]. At the same time, the chemical compositions and components of gas mixture will affect the gas transport. Therefore, the study of multi-scale flow mechanism of gas mixture is helpful to enrich people's understanding of the basic fluid transfer process, and has important practical significance and application background.

There are two ways to study multi-scale flow of gas mixture. One is the coupling method [5,6] of traditional computational fluid dynamics (CFD) method based on Euler/Navier-Stokes (Euler/N-S) equation and discrete velocity method/direct simulation Monte Carlo (DVM/DSMC) method based on Boltzmann equation. Since it is a coupling method in nature, both the accuracy and stability need to be considered when designing coupling ideas, and the problem of statistical fluctuation caused by DSMC method always exists. The other is a unified method [7–15] based on gas-kinetic theory, which aims to use one method to simulate the multi-scale flow problem in the whole regimes. Among them, Wang et al. [7] developed a unified gas kinetic scheme for two-component gas mixture based on the AAP model [16], and simulated the whole regimes flow problem of two-component gas mixture composed of Hard Sphere (HS) molecules. Zhang et al. [8, 9] developed a discrete unified gas kinetic scheme for two-component gas mixture based on the AAP model and McCormack model [17], and analyzed and compared the two kinetic models. According to Zhang's research, McCormack model is suitable for low velocity or small gradient driven (pressure, temperature, concentration) flow problems, and AAP model can effectively simulate the high-speed flow problem of two-component gas mixture. Wu et al. [10] developed a gas-kinetic unified algorithm for chemical reactions of multi-component gas mixture, and carried out the algorithm verification, and the effect is very good. Xu et al. [13, 14] developed a unified gas-kinetic scheme for multiscale and multicomponent flow transport based on AAP model.

In the past two decades, the gas-kinetic unified algorithm proposed by Li [18–20] for the whole regimes flow of single-component gases has been greatly developed and applied. At present, numerical models and algorithms considering thermodynamic non-equilibrium effects (including rotational energy excitation, continuous energy level vibrational energy excitation and discrete quantum energy level vibrational energy excitation) [21–23] and thermochemical non-equilibrium effects [24] have been developed. Combined with large-scale parallel computing platform [25], it is widely used in microchannel flow [26], external force driven flow [27], high-altitude aircraft flow around [28] and other fields. According to the characteristics of AAP model, which can effectively simulate the high-speed flow problem of two-component gas mixture and has simple structure, and is easy to be extended to multi-component gas mixture, this paper develops a gas-kinetic unified algorithm of multi-component monatomic gas mixture based on AAP model, and applies it to the study of engine vacuum plume problem.

The structure of this paper is arranged as follows: Section I introduces the relevant background, and Section 2 introduces the computable modeling of Boltzmann equation

for multi-component monatomic gas mixture. Section 3 is the verification and analysis of the algorithm. The steady normal shock wave structure, flow around two-dimensional circular cylinder and pressure/temperature gradient driven microchannel flow problems for two-component gas mixture are used to verify the reliability of the algorithm, and the internal and external mixed flow simulation study is carried out by taking the two-dimensional profile nozzle of 25N attitude control engine as the object. Section 4 is the conclusion.

2 Boltzmann equation computable modeling for multi-component monatomic gas mixture

2.1 Kinetic model equation for multi-component monatomic gas mixture

Assuming that the number of components of gas mixture is K and the velocity distribution function of gas molecules of α-th component is f_α. According to the single relaxation AAP model proposed by Andries et al. [16], the Boltzmann model equation describing the flow of multi-component monatomic gas mixture is obtained as

$$\frac{\partial f_\alpha}{\partial t}+\boldsymbol{V}\cdot\frac{\partial f_\alpha}{\partial \boldsymbol{x}}=\nu_\alpha(F_m^\alpha-f_\alpha), \tag{2.1}$$

where

$$F_m^\alpha=n^{(\alpha)}\left(\frac{m_\alpha}{2\pi k_{\mathrm{B}}T_\alpha}\right)^{\frac{3}{2}}\exp\left(-\frac{m_\alpha|\boldsymbol{V}-\boldsymbol{U}_\alpha|^2}{2k_{\mathrm{B}}T_\alpha}\right), \tag{2.2}$$

$$\nu_\alpha=\sum_{\beta=1}^{K}n^{(\beta)}\nu_{\alpha\beta}, \tag{2.3}$$

$$m_\alpha\nu_\alpha\boldsymbol{U}_\alpha=m_\alpha\nu_\alpha\boldsymbol{U}^{(\alpha)}+\sum_{\beta=1}^{K}2m_{\alpha\beta}\nu_{\alpha\beta}n^{(\beta)}\left[\boldsymbol{U}^{(\beta)}-\boldsymbol{U}^{(\alpha)}\right], \tag{2.4}$$

$$\begin{aligned}\nu_\alpha\varepsilon_\alpha=&\nu_\alpha\varepsilon^{(\alpha)}-\frac{m_\alpha\nu_\alpha}{2}\left|\boldsymbol{U}_\alpha-\boldsymbol{U}^{(\alpha)}\right|^2\\&+\sum_{\beta=1}^{K}\frac{4m_{\alpha\beta}\nu_{\alpha\beta}n^{(\beta)}}{m_\alpha+m_\beta}\left[\varepsilon^{(\beta)}-\varepsilon^{(\alpha)}+m_\beta\frac{\left|\boldsymbol{U}^{(\beta)}-\boldsymbol{U}^{(\alpha)}\right|^2}{2}\right],\end{aligned} \tag{2.5}$$

$$\varepsilon_\alpha=\frac{3}{2}k_{\mathrm{B}}T_\alpha, m_{\alpha\beta}=\frac{m_\alpha m_\beta}{m_\alpha+m_\beta}, \tag{2.6}$$

$$\nu_{\alpha\beta}=\begin{cases}\dfrac{4\sqrt{\pi}}{3}\left(\dfrac{d_\alpha+d_\beta}{2}\right)^2\sqrt{\dfrac{2k_{\mathrm{B}}T^{(\alpha)}}{m_\alpha}+\dfrac{2k_{\mathrm{B}}T^{(\beta)}}{m_\beta}}, & \text{Hard sphere,}\\ 0.422\pi\sqrt{\dfrac{a_{\alpha\beta}\left(m_\alpha+m_\beta\right)}{m_\alpha m_\beta}}, & \text{Maxwell,}\end{cases} \tag{2.7}$$

$a_{\alpha\beta}$ is proportionality constant, which is defined by

$$a_{\alpha\beta}=4r^4\psi_{\alpha\beta}, \tag{2.8}$$

where $\psi_{\alpha\beta}$ denotes interaction potential energy of two particles with mass m_α and mass m_β and distance r, respectively.

Assuming that the molecular velocities of all gas components are in the same value range, the macroscopic flow parameter expressions of α-th component are

$$n^{(\alpha)}=\int_{-\infty}^{+\infty}f_\alpha \mathrm{d}\boldsymbol{V},\rho^{(\alpha)}=m_\alpha n^{(\alpha)},n^{(\alpha)}\boldsymbol{U}^{(\alpha)}=\int_{-\infty}^{+\infty}\boldsymbol{V}f_\alpha \mathrm{d}\boldsymbol{V}, \tag{2.9}$$

$$\frac{3}{2}n^{(\alpha)}k_{\mathrm{B}}T^{(\alpha)}=\frac{1}{2}\int_{-\infty}^{+\infty}m_\alpha\left|\boldsymbol{V}-\boldsymbol{U}^{(\alpha)}\right|^2 f_\alpha \mathrm{d}\boldsymbol{V}, \tag{2.10}$$

$$p^{(\alpha)}=n^{(\alpha)}k_{\mathrm{B}}T^{(\alpha)}, \tag{2.11}$$

$$P_{ij}^{(\alpha)}=\int_{-\infty}^{+\infty}m_\alpha\left(V_i-U_i^{(\alpha)}\right)\left(V_j-U_j^{(\alpha)}\right)f_\alpha \mathrm{d}\boldsymbol{V}, \tag{2.12}$$

$$\boldsymbol{q}^{(\alpha)}=\frac{1}{2}\int_{-\infty}^{+\infty}m_\alpha\left(\boldsymbol{V}-\boldsymbol{U}^{(\alpha)}\right)\left|\boldsymbol{V}-\boldsymbol{U}^{(\alpha)}\right|^2 f_\alpha \mathrm{d}\boldsymbol{V}, \tag{2.13}$$

where n is the number density, ρ is the density, V is the molecular velocity, U is the average velocity, T is the temperature, p is the pressure, P_{ij} is the stress tensor, and q is the heat flux.

The relationships between the macroscopic flow variables of α-th component and the total macroscopic flow variables of gas mixture are

$$n=\sum_\alpha n^{(\alpha)},\rho=\sum_\alpha m_\alpha n^{(\alpha)},\rho\boldsymbol{U}=\sum_\alpha\int_{-\infty}^{+\infty}m_\alpha\boldsymbol{V}f_\alpha \mathrm{d}\boldsymbol{V}, \tag{2.14}$$

$$p=nk_{\mathrm{B}}T=\sum_\alpha\left(n^{(\alpha)}k_{\mathrm{B}}T^{(\alpha)}+\frac{1}{3}\rho^{(\alpha)}\left|\boldsymbol{U}^{(\alpha)}-\boldsymbol{U}\right|^2\right), \tag{2.15}$$

$$P_{ij}=\sum_\alpha\left(P_{ij}^{(\alpha)}+\rho^{(\alpha)}\left(\boldsymbol{U}^{(\alpha)}-\boldsymbol{U}\right)^2\right), \tag{2.16}$$

$$\begin{aligned}q_i=\sum_\alpha\Bigg(&q_i^{(\alpha)}+\sum_j\left(P_{ij}^{(\alpha)}\left(U_j^{(\alpha)}-U_j\right)\right)+\frac{3}{2}p^{(\alpha)}\left(\boldsymbol{U}^{(\alpha)}-\boldsymbol{U}\right)\\&+\frac{1}{2}\rho^{(\alpha)}\left(\boldsymbol{U}^{(\alpha)}-\boldsymbol{U}\right)\left|\boldsymbol{U}^{(\alpha)}-\boldsymbol{U}\right|^2\Bigg),\end{aligned} \tag{2.17}$$

where i and j represent x, y and z.

In order to eliminate the scale difference between the velocity distribution function and the macroscopic flow, the model equation is made dimensionless. Taking the average molecular mass and diameter of gas mixture as the reference mass and reference diameter, the average number density and temperature of gas mixture as the reference number density and reference temperature, and other reference quantities similar to the single component, the dimensionless Boltzmann model equation describing the flow of the multi-component monatomic gas mixture is finally obtained

$$\frac{\partial \widetilde{f}_\alpha}{\partial \widetilde{t}}+\widetilde{\boldsymbol{V}}\cdot\frac{\partial \widetilde{f}_\alpha}{\partial \widetilde{\boldsymbol{x}}}=\widetilde{\nu}_\alpha\left(\widetilde{F}_m^\alpha-\widetilde{f}_\alpha\right), \tag{2.18}$$

where

$$\widetilde{F}_m^\alpha=\widetilde{n}^{(\alpha)}\left(\frac{\widetilde{m}_\alpha}{\pi\widetilde{T}_\alpha}\right)^{\frac{3}{2}}\exp\left(-\frac{\widetilde{m}_\alpha\left|\widetilde{\boldsymbol{V}}-\widetilde{\boldsymbol{U}}_\alpha\right|^2}{\widetilde{T}_\alpha}\right), \tag{2.19}$$

$$\widetilde{\nu}_\alpha=\sum_{\beta=1}^{K}\widetilde{n}^{(\beta)}\widetilde{\nu}_{\alpha\beta}, \tag{2.20}$$

$$\widetilde{\boldsymbol{U}}_\alpha=\widetilde{\boldsymbol{U}}^{(\alpha)}+\frac{1}{\widetilde{m}_\alpha\widetilde{\nu}_\alpha}\sum_{\beta=1}^{K}2\widetilde{m}_{\alpha\beta}\widetilde{\nu}_{\alpha\beta}\widetilde{n}^{(\beta)}\left[\widetilde{\boldsymbol{U}}^{(\beta)}-\widetilde{\boldsymbol{U}}^{(\alpha)}\right], \tag{2.21}$$

$$\begin{aligned}\widetilde{T}_\alpha=&\widetilde{T}^{(\alpha)}-\frac{2\widetilde{m}_\alpha}{3}\left|\widetilde{\boldsymbol{U}}_\alpha-\widetilde{\boldsymbol{U}}^{(\alpha)}\right|^2\\&+\frac{1}{\widetilde{\nu}_\alpha}\sum_{\beta=1}^{K}\frac{4\widetilde{m}_{\alpha\beta}\widetilde{\nu}_{\alpha\beta}\widetilde{n}^{(\beta)}}{\widetilde{m}_\alpha+\widetilde{m}_\beta}\left[\widetilde{T}^{(\beta)}-\widetilde{T}^{(\alpha)}+\frac{2}{3}\widetilde{m}_\beta\left|\widetilde{\boldsymbol{U}}^{(\beta)}-\widetilde{\boldsymbol{U}}^{(\alpha)}\right|^2\right],\end{aligned} \tag{2.22}$$

$$\widetilde{\nu}_{\alpha\beta}=\begin{cases}\dfrac{4\sqrt{\pi}}{3}\left(\dfrac{\widetilde{d}_\alpha+\widetilde{d}_\beta}{2}\right)^2\sqrt{\dfrac{\widetilde{T}^{(\alpha)}}{\widetilde{m}_\alpha}+\dfrac{\widetilde{T}^{(\beta)}}{\widetilde{m}_\beta}},\\ \cdot\displaystyle\sum_{l=1}^{K}\left(\frac{\widetilde{n}_\infty^{(l)}}{Kn_\infty}\left(\sum_{\sigma=1}^{K}\left(\pi\left(\frac{\widetilde{d}_l+\widetilde{d}_\sigma}{2}\right)^2\widetilde{n}_\sigma\sqrt{1+\frac{\widetilde{m}_l}{\widetilde{m}_\sigma}}\right)\right)^{-1}\right),\\ 0.422\pi\sqrt{\dfrac{\widetilde{a}_{\alpha\beta}\left(\widetilde{m}_\alpha+\widetilde{m}_\beta\right)}{\widetilde{m}_\alpha\widetilde{m}_\beta}},\end{cases} \tag{2.23}$$

where n_∞ is mole fraction of incoming component, d is molecular diameter of gas component, m is molecular mass of gas component and Kn_∞ is incoming Knudsen number.

The dimensionless macroscopic flow parameter expressions of α-th component are

$$\widetilde{n}^{(\alpha)}=\int_{-\infty}^{+\infty}\widetilde{f}_\alpha\mathrm{d}\widetilde{\boldsymbol{V}},\quad \widetilde{\rho}^{(\alpha)}=\widetilde{m}_\alpha\widetilde{n}^{(\alpha)},\quad \widetilde{n}^{(\alpha)}\widetilde{\boldsymbol{U}}^{(\alpha)}=\int_{-\infty}^{+\infty}\widetilde{\boldsymbol{V}}\widetilde{f}_\alpha\mathrm{d}\widetilde{\boldsymbol{V}}, \tag{2.24}$$

$$\frac{3}{2}\widetilde{n}^{(\alpha)}\widetilde{T}^{(\alpha)}=\int_{-\infty}^{+\infty}\widetilde{m}_\alpha\left|\widetilde{\boldsymbol{V}}-\widetilde{\boldsymbol{U}}^{(\alpha)}\right|^2\widetilde{f}_\alpha\mathrm{d}\widetilde{\boldsymbol{V}},\tag{2.25}$$

$$\widetilde{p}^{(\alpha)}=\widetilde{n}^{(\alpha)}\widetilde{T}^{(\alpha)},\tag{2.26}$$

$$27\widetilde{P}_{ij}^{(\alpha)}=2\int_{-\infty}^{+\infty}\widetilde{m}_\alpha\left(\widetilde{V}_i-\widetilde{U}_i^{(\alpha)}\right)\left(\widetilde{V}_j-\widetilde{U}_j^{(\alpha)}\right)\widetilde{f}_\alpha\mathrm{d}\widetilde{\boldsymbol{V}},\tag{2.27}$$

$$\widetilde{\boldsymbol{q}}^{(\alpha)}=\int_{-\infty}^{+\infty}\widetilde{m}_\alpha\left(\widetilde{\boldsymbol{V}}-\widetilde{\boldsymbol{U}}^{(\alpha)}\right)\left|\widetilde{\boldsymbol{V}}-\widetilde{\boldsymbol{U}}^{(\alpha)}\right|^2\widetilde{f}_\alpha\mathrm{d}\widetilde{\boldsymbol{V}}.\tag{2.28}$$

The relationships between the dimensionless macroscopic flow variables of α-th component and the total dimensionless macroscopic flow variables of gas mixture are

$$\widetilde{n}=\sum_\alpha\widetilde{n}^{(\alpha)},\quad\widetilde{\rho}=\sum_\alpha\widetilde{m}_\alpha\widetilde{n}^{(\alpha)},\quad\widetilde{\rho}\widetilde{\boldsymbol{U}}=\sum_\alpha\int_{-\infty}^{+\infty}\widetilde{m}_\alpha\widetilde{\boldsymbol{V}}\widetilde{f}_\alpha\mathrm{d}\widetilde{\boldsymbol{V}},\tag{2.29}$$

$$\widetilde{p}=\widetilde{n}\widetilde{T}=\sum_\alpha\left(\widetilde{n}^{(\alpha)}\widetilde{T}^{(\alpha)}+\frac{2}{3}\widetilde{\rho}^{(\alpha)}\left|\widetilde{\boldsymbol{U}}^{(\alpha)}-\widetilde{\boldsymbol{U}}\right|^2\right),\tag{2.30}$$

$$\widetilde{P}_{ij}=\sum_\alpha\left(\widetilde{P}_{ij}^{(\alpha)}+2\widetilde{\rho}^{(\alpha)}\left(\widetilde{\boldsymbol{U}}^{(\alpha)}-\widetilde{\boldsymbol{U}}\right)^2\right),\tag{2.31}$$

$$\widetilde{q}_i=\sum_\alpha\left\{\widetilde{q}_i^{(\alpha)}+\sum_j\left(\widetilde{P}_{ij}^{(\alpha)}\left(\widetilde{U}_j^{(\alpha)}-\widetilde{U}_j\right)\right)+\frac{3}{2}\widetilde{p}^{(\alpha)}\left(\widetilde{\boldsymbol{U}}^{(\alpha)}-\widetilde{\boldsymbol{U}}\right)\right.$$
$$\left.+\widetilde{\rho}^{(\alpha)}\left(\widetilde{\boldsymbol{U}}^{(\alpha)}-\widetilde{\boldsymbol{U}}\right)\left|\widetilde{\boldsymbol{U}}^{(\alpha)}-\widetilde{\boldsymbol{U}}\right|^2\right\}.\tag{2.32}$$

2.2 Gas-kinetic unified algorithm

2.2.1 Reduced velocity distribution functions for two-dimensional gas flow problems

For two-dimensional gas flow problems, the reduced velocity distribution function can be introduced to eliminate the dependence of original velocity distribution function on the molecular velocity V_z, further simplifying the solution process and the demand for computer storage. For Boltzmann model equation (2.18) for multi-component monatomic gas mixture, the function $\widetilde{g}_{\alpha i}\left(\widetilde{x},\widetilde{y},\widetilde{V}_x,\widetilde{V}_y,\widetilde{t}\right)$ is introduced

$$\widetilde{g}_{\alpha1}=\int\widetilde{f}_\alpha\mathrm{d}\widetilde{V}_z,\quad\widetilde{g}_{\alpha2}=\int V_z^2\widetilde{f}_\alpha\mathrm{d}\widetilde{V}_z.\tag{2.33}$$

By integrating Eq. (2.18) with weight factor 1 and $\widetilde{V}_z^2$ in infinite intervals, the continuous dependence on velocity component $\widetilde{V}_z$ is eliminated, and the model equations of reduced velocity distribution functions $\widetilde{g}_{\alpha1}$ and $\widetilde{g}_{\alpha2}$ are obtained

$$\begin{cases}\dfrac{\partial\widetilde{g}_{\alpha1}}{\partial\widetilde{t}}+\widetilde{\boldsymbol{V}}\cdot\dfrac{\partial\widetilde{g}_{\alpha1}}{\partial\widetilde{\boldsymbol{x}}}=\widetilde{\nu}_\alpha\left(\widetilde{G}_m^{\alpha1}-\widetilde{g}_{\alpha1}\right),\\[2ex]\dfrac{\partial\widetilde{g}_{\alpha2}}{\partial\widetilde{t}}+\widetilde{\boldsymbol{V}}\cdot\dfrac{\partial\widetilde{g}_{\alpha2}}{\partial\widetilde{\boldsymbol{x}}}=\widetilde{\nu}_\alpha\left(\widetilde{G}_m^{\alpha2}-\widetilde{g}_{\alpha2}\right),\end{cases}\tag{2.34}$$

where

$$\widetilde{G}_m^{\alpha 1}=\widetilde{n}^{(\alpha)}\frac{\widetilde{m}_\alpha}{\pi\widetilde{T}_\alpha}\exp\left(-\frac{\widetilde{m}_\alpha\left[\left(\widetilde{V}_x-\widetilde{U}_{\alpha x}\right)^2+\left(\widetilde{V}_y-\widetilde{U}_{\alpha y}\right)^2\right]}{\widetilde{T}_\alpha}\right), \tag{2.35}$$

$$\widetilde{G}_m^{\alpha 2}=\frac{\widetilde{T}_\alpha\widetilde{G}_m^{\alpha 1}}{2\widetilde{m}_\alpha}. \tag{2.36}$$

The dimensionless macroscopic flow parameters of α-th component expressed by $\widetilde{g}_{\alpha 1}$ and $\widetilde{g}_{\alpha 2}$ are

$$\widetilde{n}^{(\alpha)}=\iint\widetilde{g}_{\alpha 1}\mathrm{d}\widetilde{V}_x\mathrm{d}\widetilde{V}_y, \tag{2.37}$$

$$\widetilde{\rho}^{(\alpha)}=\widetilde{m}_\alpha\widetilde{n}^{(\alpha)},\quad \widetilde{n}^{(\alpha)}\widetilde{\boldsymbol{U}}^{(\alpha)}=\iint\widetilde{\boldsymbol{V}}\widetilde{g}_{\alpha 1}\mathrm{d}\widetilde{V}_x\mathrm{d}\widetilde{V}_y, \tag{2.38}$$

$$\frac{3}{2}\widetilde{n}^{(\alpha)}\widetilde{T}^{(\alpha)}+\widetilde{m}_\alpha\widetilde{n}^{(\alpha)}{\widetilde{U}^{(\alpha)}}^2=\iint\widetilde{m}_\alpha\left[\left(\widetilde{V}_x^2+\widetilde{V}_y^2\right)\widetilde{g}_{\alpha 1}+\widetilde{g}_{\alpha 2}\right]\mathrm{d}\widetilde{V}_x\mathrm{d}\widetilde{V}_y, \tag{2.39}$$

$$\widetilde{p}^{(\alpha)}=\widetilde{n}^{(\alpha)}\widetilde{T}^{(\alpha)}, \tag{2.40}$$

$$\widetilde{P}_{ij}^{(\alpha)}=2\iint\widetilde{m}_\alpha\left(\widetilde{V}_i-\widetilde{U}_i^{(\alpha)}\right)\left(\widetilde{V}_j-\widetilde{U}_j^{(\alpha)}\right)\widetilde{g}_{\alpha 1}\mathrm{d}\widetilde{V}_x\mathrm{d}\widetilde{V}_y, \tag{2.41}$$

$$\begin{aligned}\widetilde{\boldsymbol{q}}^{(\alpha)}=&\iint\widetilde{m}_\alpha\left(\widetilde{\boldsymbol{V}}-\widetilde{\boldsymbol{U}}^{(\alpha)}\right)\\&\cdot\left[\left(\left(\left(\widetilde{V}_x-\widetilde{U}_x^{(\alpha)}\right)^2+\left(\widetilde{V}_y-\widetilde{U}_y^{(\alpha)}\right)^2\right)\widetilde{g}_{\alpha 1}+\widetilde{g}_{\alpha 2}\right)\mathrm{d}\widetilde{V}_x\mathrm{d}\widetilde{V}_y\right].\end{aligned} \tag{2.42}$$

2.2.2 Wall boundary condition

For two-dimensional gas flow problems that considering multi-component monatomic gas mixture, the wall boundary conditions of completely diffuse reflection model is

$$\begin{aligned}\widetilde{g}_{\alpha 1,\mathrm{w}}&=\widetilde{n}_{\mathrm{w}}^{(\alpha)}\frac{\widetilde{m}_\alpha}{\pi\widetilde{T}_{\mathrm{w}}}\exp\left(-\frac{\widetilde{m}_\alpha\left(\widetilde{V}_x^2+\widetilde{V}_y^2\right)}{\widetilde{T}_{\mathrm{w}}}\right),\\\widetilde{g}_{\alpha 2,\mathrm{w}}&=\frac{\widetilde{T}_{\mathrm{w}}}{2\widetilde{m}_\alpha}\widetilde{g}_{\alpha 1,\mathrm{w}},\end{aligned} \tag{2.43}$$

where

$$\widetilde{n}_{\mathrm{w}}^{(\alpha)}=-2\sqrt{\frac{\pi\widetilde{m}_\alpha}{\widetilde{T}_{\mathrm{w}}}}\iint_{\widetilde{C}_n<0}\widetilde{C}_n\widetilde{g}_{\alpha 1}\mathrm{d}\widetilde{V}_x\mathrm{d}\widetilde{V}_y. \tag{2.44}$$

When $\widetilde{C}_n>0$, the velocity distribution functions of gas molecules on the wall are given by Eq. (2.43). When $\widetilde{C}_n<0$, the velocity distribution functions of gas molecules on the wall are given by using second-order upwind-difference approximations from the adjacent grids in the flow field. Where $\widetilde{C}_n=\widetilde{\boldsymbol{V}}\cdot\widetilde{\boldsymbol{n}}$, $\boldsymbol{n}$ is the wall unit normal vector, which points from the wall to the interior of the fluid.

2.2.3 Finite difference scheme

For the Boltzmann model equation of multi-component monatomic gas mixture, the model equation (2.34) is transformed into a hyperbolic conservation equation at each discrete velocity coordinate point independent of each other by using the conservation discrete velocity coordinate method. Through coordinate transformation, the discrete hyperbolic conservation model equation is transformed from physical plane to computational plane, and its matrix form is

$$\frac{\partial \widetilde{\boldsymbol{Q}}}{\partial \widetilde{t}}+\frac{\partial \widetilde{\boldsymbol{F}}}{\partial \xi}+\frac{\partial \widetilde{\boldsymbol{G}}}{\partial \eta}=\widetilde{\boldsymbol{S}}, \tag{2.45}$$

where

$$\widetilde{\boldsymbol{Q}}=\widetilde{J}\begin{pmatrix} \widetilde{g}_{\alpha 1,\sigma,\delta}\left(\widetilde{x},\widetilde{y},\widetilde{t}\right) \\ \widetilde{g}_{\alpha 2,\sigma,\delta}\left(\widetilde{x},\widetilde{y},\widetilde{t}\right) \end{pmatrix}, \quad \widetilde{\boldsymbol{F}}=\widetilde{\bar{U}}\widetilde{\boldsymbol{Q}}, \quad \widetilde{\boldsymbol{G}}=\widetilde{\bar{V}}\widetilde{\boldsymbol{Q}}, \tag{2.46}$$

$$\widetilde{\boldsymbol{S}}=\widetilde{J}\begin{pmatrix} \widetilde{\nu}_{\alpha}\left(\widetilde{G}_{m}^{\alpha 1,\sigma,\delta}-\widetilde{g}_{\alpha 1,\sigma,\delta}\right) \\ \widetilde{\nu}_{\alpha}\left(\widetilde{G}_{m}^{\alpha 2,\sigma,\delta}-\widetilde{g}_{\alpha 2,\sigma,\delta}\right) \end{pmatrix}, \tag{2.47}$$

$$\widetilde{J}=\frac{\partial(\widetilde{x},\widetilde{y})}{\partial(\xi,\eta)}=\widetilde{x}_{\xi}\widetilde{y}_{\eta}-\widetilde{y}_{\xi}\widetilde{x}_{\eta}, \tag{2.48}$$

$$\widetilde{\xi}_{x}=\frac{\widetilde{y}_{\eta}}{\widetilde{J}}, \quad \widetilde{\xi}_{y}=-\frac{\widetilde{x}_{\eta}}{\widetilde{J}}, \quad \widetilde{\eta}_{x}=-\frac{\widetilde{y}_{\xi}}{\widetilde{J}}, \quad \widetilde{\eta}_{y}=\frac{\widetilde{x}_{\xi}}{\widetilde{J}}, \tag{2.49}$$

$$\widetilde{\bar{U}}_{x}=\widetilde{\bar{V}}_{x\sigma}\widetilde{\xi}_{x}+\widetilde{\bar{V}}_{y\delta}\widetilde{\xi}_{y}, \quad \widetilde{\bar{U}}_{y}=\widetilde{\bar{V}}_{x\sigma}\widetilde{\eta}_{x}+\widetilde{\bar{V}}_{y\delta}\widetilde{\eta}_{y}. \tag{2.50}$$

Using the unsteady time splitting method, the model equation (2.45) is split into the convective motion equations and the collision relaxation source term equation for coupling solution

$$\frac{\partial \widetilde{\boldsymbol{Q}}}{\partial \widetilde{t}}=\widetilde{\boldsymbol{S}}, \tag{2.51}$$

$$\frac{\partial \widetilde{\boldsymbol{Q}}}{\partial \widetilde{t}}+\frac{\partial \widetilde{\boldsymbol{F}}}{\partial \xi}=0, \tag{2.52}$$

$$\frac{\partial \widetilde{\boldsymbol{Q}}}{\partial \widetilde{t}}+\frac{\partial \widetilde{\boldsymbol{G}}}{\partial \eta}=0. \tag{2.53}$$

The collision relaxation source term equation is solved analytically and the convective equations of motion are discretized using the NND scheme [29], which finally leads to the following finite difference numerical scheme

$$\widetilde{Q}^{(n+1)}=L_{s}\left(\Delta\widetilde{t}/2\right)L_{\xi}\left(\Delta\widetilde{t}/2\right)L_{\eta}\left(\Delta\widetilde{t}\right)L_{\xi}\left(\Delta\widetilde{t}/2\right)L_{s}\left(\Delta\widetilde{t}/2\right)\widetilde{Q}^{(n)}. \tag{2.54}$$

The time step is given by the scheme stability condition

$$\Delta\widetilde{t}=CFL/\max\left(\frac{\left|\widetilde{\bar{U}}_{x}\right|}{\Delta\xi},\frac{\left|\widetilde{\bar{U}}_{y}\right|}{\Delta\eta}\right). \tag{2.55}$$

3 Verification and analysis

The steady normal shock wave structure, flow around two-dimensional circular cylinder and pressure/temperature gradient driven microchannel flow problems for two-component gas mixture are used to verify the reliability of the algorithm. And direct at 25N attitude control engine, the two-dimensional profile nozzle internal and external mixed flow simulation is carried out.

3.1 Steady normal shock wave structure problem for two-component gas mixture

Consider a steady normal shock wave structure problem for two-component gas mixture (the mixture of component 1 and component 2). The mole fraction of component 1 helium (He) is set to 0.97, the molecular mass is $6.65\times10^{-27}kg$, and the diameter is $2.193\times10^{-10}m$. The mole fraction of component 2 xenon (Xe) is set to 0.03, the molecular mass is $2.18\times10^{-25}kg$, and the diameter is $4.939\times10^{-10}m$. The Mach number of gas mixture is 3.89, the Mach number of component 1 helium is 2.783, and the Mach number of component 2 xenon is 15.932. This example belongs to a shock wave structure problem of two-component gas mixture with large mass ratio and large mole fraction ratio, which has certain challenges for the algorithm and model. For convenience, the nondimensional symbol "$\sim$" is omitted.

Fig. 1 shows the density and temperature shock wave structures of each component in the gas mixture, where the values calculated in this paper are compared with the re-

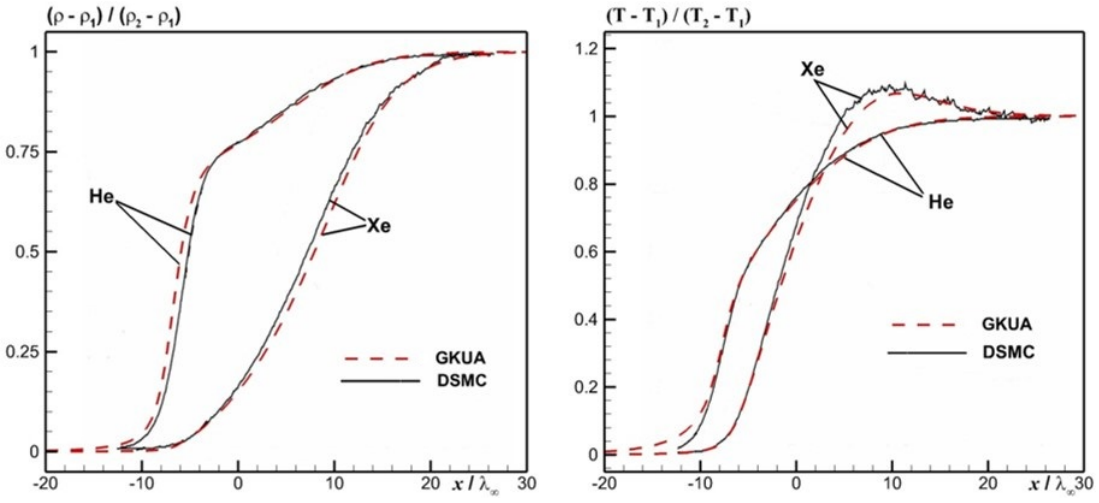

(a) Density profile (b) Temperature profile

Figure 1: Density and temperature shock wave structures of each component in the gas mixture.

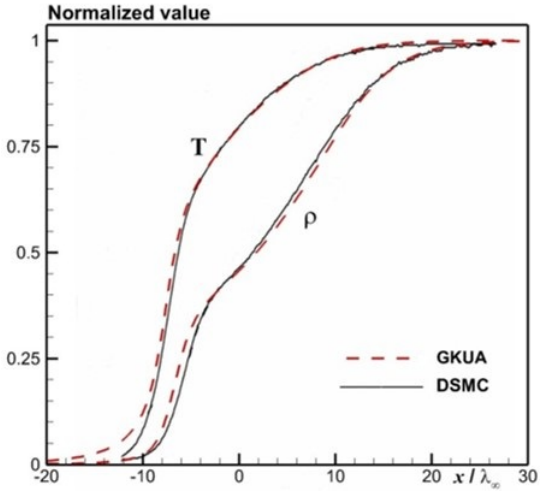

Figure 2: Density and temperature shock wave structures of gas mixture.

sults obtained by the DSMC method [30]. It can be seen from the figure that the change trend of the shock wave structure obtained by the two methods is basically the same, with only minor differences. Comparing the temperature profiles of the components He and Xe, it is found that the temperature profile of Xe shows a clear bulge in the downstream. Fig. 2 shows the density and temperature shock wave structures of gas mixture, where the values calculated in this paper are compared with the results obtained by the DSMC method. It can be seen from the figure that the results of the two methods are in good agreement. The temperature profile of gas mixture does not show a bulge in the downstream, which is different from the temperature profile of the component Xe. From the perspective of the change trend, the gradients of the density and temperature of gas mixture are larger in the upstream and smoother in the downstream.

Fig. 3 shows the mole fraction comparison curve of component Xe in the gas mixture, and the curve calculated in this paper is in good agreement with those obtained by the DSMC method. Fig. 4 shows the diffusion velocity comparison curves of component He and component Xe in the gas mixture, from which it can be seen that the velocity of component Xe in the gas mixture is larger than the average velocity of gas mixture, and the velocity of component He is smaller than the average velocity of gas mixture. The results show that the unified algorithm developed in this paper can deal with the steady normal shock wave structure problem well.

3.2 Flow around two-dimensional circular cylinder for two-component gas mixture

Consider a helium-argon (He-Ar) gas mixture flow around two-dimensional circular cylinder. The temperature of incoming flow is set to $200K$, wall temperature is set to

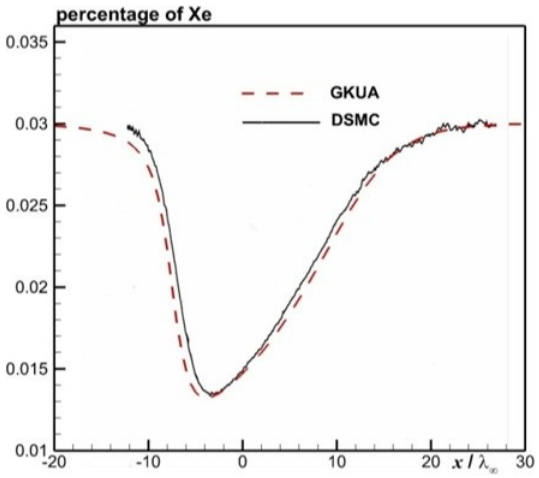

Figure 3: Mole fraction comparison curve of component Xe in the gas mixture.

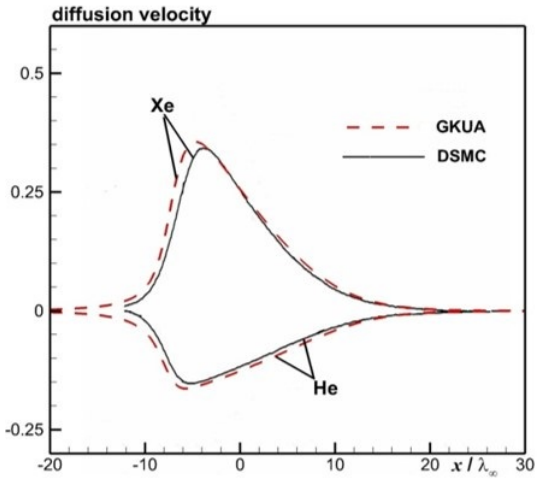

Figure 4: Diffusion velocity comparison curves of components He and Xe in the gas mixture.

$300K$, Knudsen number of incoming flow is set to 0.01, Mach number of incoming flow is set to 3. Three different mole fraction states are set, as shown in the following table, where the number density of incoming flow in state 1 is $1.8046\times10^{20}/m^3$, the number density of incoming flow in state 2 is $2.69\times10^{20}/m^3$, and the number density of incoming flow in state 3 is $4.1974\times10^{20}/m^3$. For convenience, the nondimensional symbol "$\sim$" is omitted. The reference temperature is the temperature of incoming flow. In the space, the total number of grid is 3321, the particle velocity space is discretized with 32×32 mesh points based on Gauss-Hermite rule. When the residual is less than 1×10^{-6}, the calculation is considered to be convergent.

Table 1: Mole fraction states of gas components.

Component	State 1	State 2	State 3
He	0.1	0.5	0.9
Ar	0.9	0.5	0.1

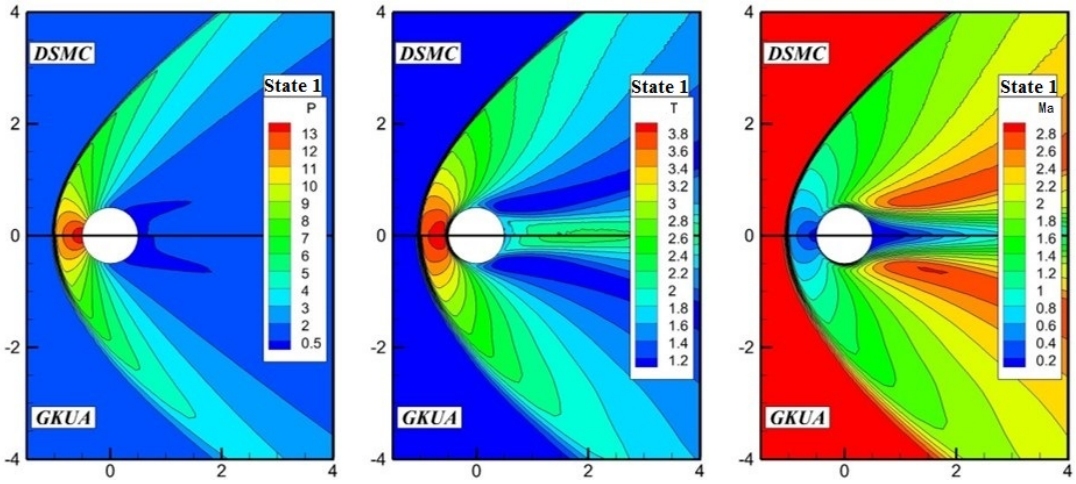

(a) Pressure (b) Temperature (c) Mach number

Figure 5: Comparison between the contour distributions of each macroscopic flow parameter of the flow field calculated by GKUA and the results obtained by DSMC at state 1.

Fig. 5 shows the comparison between the contour distributions of each macroscopic flow parameter of the flow field calculated in this paper and the results obtained by the DSMC program [31] at state 1. It can be seen from the figure that the contour distributions of each macroscopic flow parameter obtained by the two methods are basically in the situation of upper and lower symmetry, which is almost identical in the windward area, and there is only a slight difference in the leeward area. This indicates that the simulation results of the two methods are in good agreement, which confirms the reliability of the proposed algorithm.

Fig. 6 shows the mole fraction contour distributions of each component in the flow field under three different states. It can be seen from the figure that the diffusion of gas molecules is relatively obvious. In the post-wave region, the component He gradually decreases and the component Ar gradually increases. In the inner region of the shock wave, the component He gradually increases and the component Ar gradually decreases.

Fig. 7 shows the mole fraction distributions of each component on the wall for three different states. Take the zero point of the X-axis as the center, stagnation point as the starting point, and calculate the deflection Angle clockwise. It can be seen from the figure

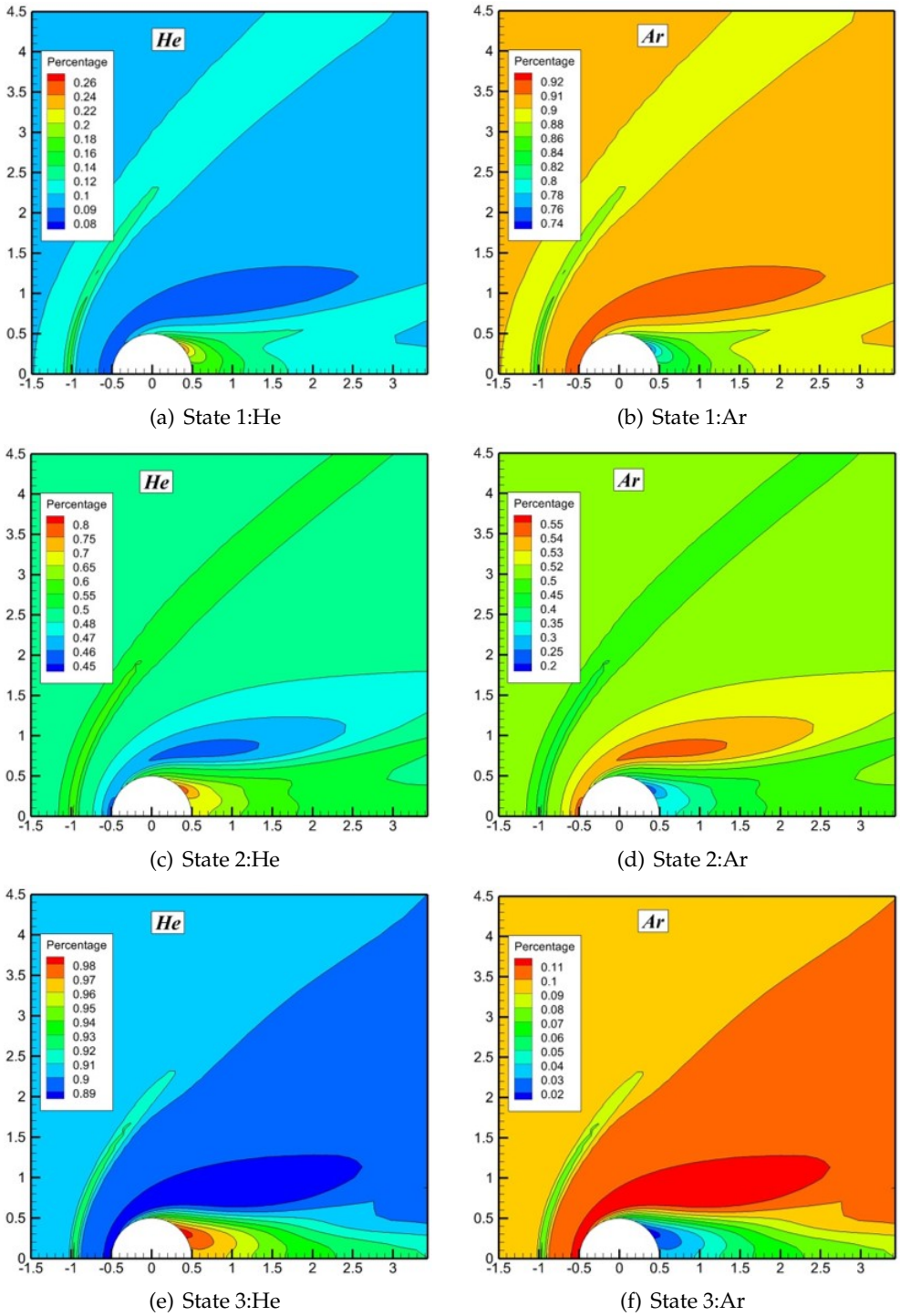

(a) State 1:He (b) State 1:Ar

(c) State 2:He (d) State 2:Ar

(e) State 3:He (f) State 3:Ar

Figure 6: Mole fraction contour distributions of each component in the flow field under three different states.

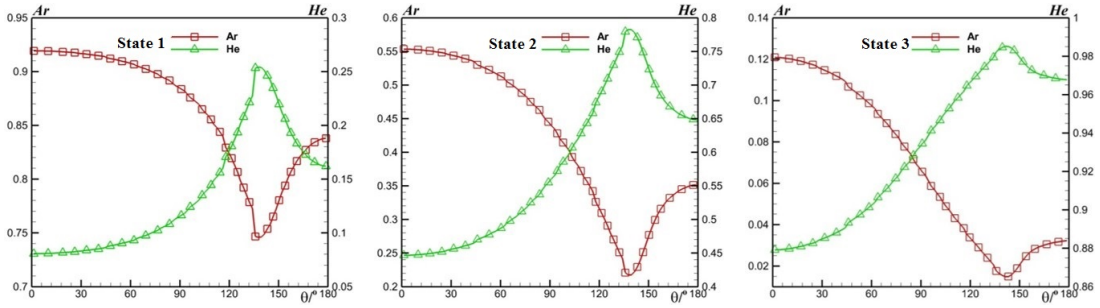

(a) State 1 (b) State 2 (c) State 3

Figure 7: Mole fraction contour distributions of each component in the flow field under three different states.

that the mole fraction of the component He at the stagnation point is lower than that in the incoming flow, and its mole fraction distribution first increases and then decreases along the wall, reaching the maximum when the deflection Angle is about 135 degrees. Under the three different mole fraction states, the mole fraction change trend of each component does not produce much change, which means that the concentration ratio does not have a significant effect on diffusion.

3.3 Gradient driven microchannel flow problem for two-component gas mixture

Consider a pressure/temperature gradient driven micro-channel flow problem [32] for two-component gas mixture. The schematic diagram of the micro-channel flow is shown in Fig. 8, where C_P and C_T are the gradient constants. The channel aspect ratio is 40, the absolute value of gradient constant is 0.01, and the gas medium is hard sphere molecule gas. The two-component molecular mass ratios m_2/m_1 are 2, 4 and 10, and the two-component molecular diameter ratio d_2/d_1 is 1. The wall boundary of the channel is the diffuse reflection boundary, and the inlet and outlet boundaries are pressure boundary. The molecular mean free path is defined as $\lambda = 1/\left(\sqrt{2}\pi n_0 d_1^2\right)$, and the Knudsen number is defined as $Kn = \lambda/H$, where n_0 is the molecular density of the inlet gas. The concentration ratio at the inlet is 1. In the pressure gradient driven flow, the dimensionless particle flux of gas component is $M_P = \frac{1}{C_P}\int_{\frac{-1}{2}}^{\frac{1}{2}} \frac{U}{\sqrt{2k_B T_0/m_1}} \mathrm{d}(y/H)$, and the flux M_T in the temperature gradient flow is defined similarly.

Fig. 9 shows the relationship between particle fluxes and Knudsen number in the pressure gradient driven flow under different component molecular mass ratios, where the reference object is the Linearized Boltzmann solution data in reference [26]. It can be seen from the figure that the particle fluxes in the pressure gradient driven flow under different component molecular mass ratios agree well with the fluxes given in reference in general. The partial deviation in the low Knudsen number region is due to the different

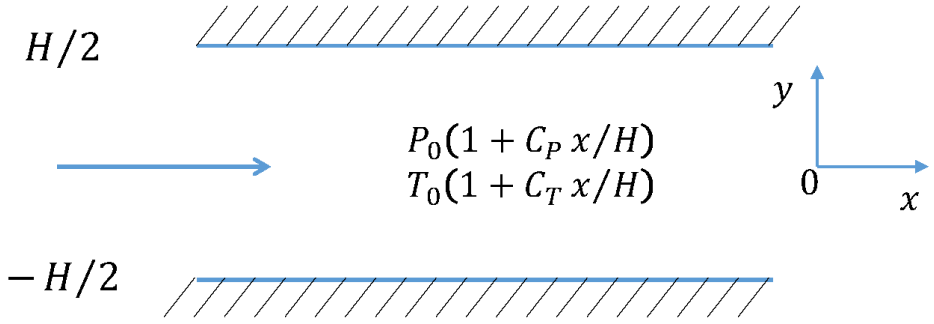

Figure 8: Schematic diagram of micro-channel flow problem.

transport coefficients recovered by different Boltzmann model equations. At the same time, the well-known phenomenon of "minimum Knudsen" [33] in the rarefied Poiseuille flow has also been observed from the pressure gradient driven flow, that is, there is a minimum of particle flux $|M_P|$ around $Kn \approx 1$.

Fig. 10 shows the relationship between particle fluxes and Knudsen number in the temperature gradient driven flow under different component molecular mass ratios. It can be seen from the figure that the fluxes of the heavy particles in the temperature gradient driven flow under different component molecular mass ratios agree well with the fluxes given by the reference [26], while the fluxes of the light component particles deviate from the fluxes given by the reference. With the increase of the molecular mass difference value between components, the difference value between the particle flux and the reference value of the light component becomes larger. It is speculated that the light component of the temperature gradient driven flow to be more sensitive to the difference of the transport coefficient.

As can be seen in Fig. 9 and Fig. 10, with the increase of Knudsen number, the flux difference between the light and heavy component particles also increases. In the case of large Knudsen number, the collision frequency between the component particles is greatly reduced, and the component particles cannot fully exchange momentum and energy, so that the velocities of components are different, and then the particle fluxes are different. In the case of small Knudsen number, the component particles collide sufficiently, and the velocities of different components are close to each other. Therefore, in the region of low Knudsen number, the flux difference between the light and heavy component particles is very small, which is consistent with the numerical simulation.

3.4 Two-dimensional profile nozzle internal and external mixed flow problem

Taking 25N attitude control engine two-dimensional profile as the object, the study for two-dimensional profile nozzle internal and external mixed flow problem is carried out,

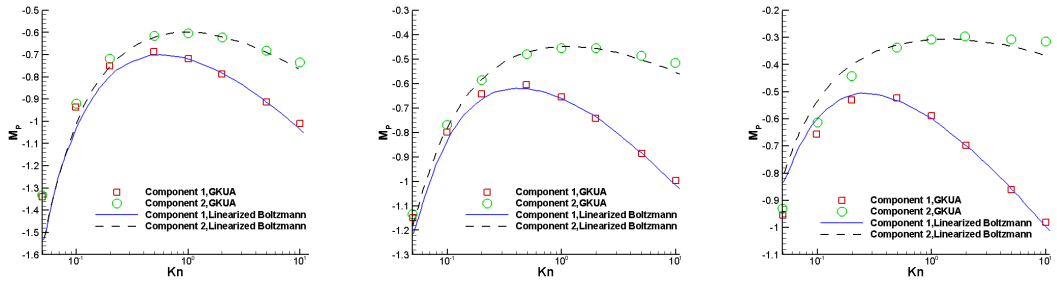

(a) $m_2/m_1=2$ (b) $m_2/m_1=4$ (c) $m_2/m_1=10$

Figure 9: Relationship between particle fluxes and Knudsen number in the pressure gradient driven flow under different component molecular mass ratios.

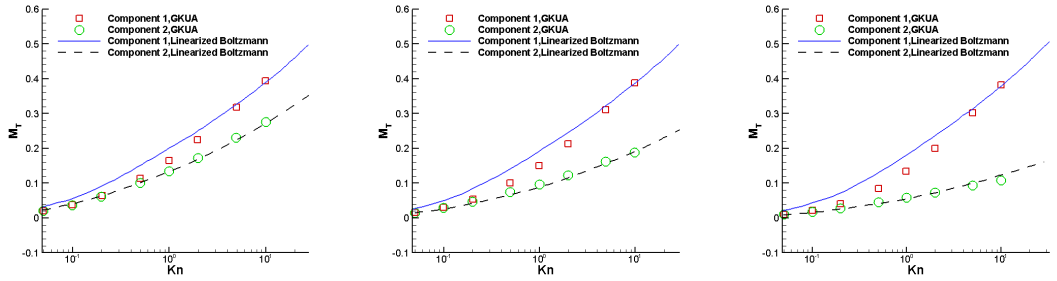

(a) $m_2/m_1=2$ (b) $m_2/m_1=4$ (c) $m_2/m_1=10$

Figure 10: Relationship between particle fluxes and Knudsen number in the temperature gradient driven flow under different component molecular mass ratios.

and the influences of the component concentration ratio and mass ratio on the molecular transport in the engine internal and external mixed flow field are discussed. In the space, the total number of grid is 4697, the particle velocity space is discretized with 32×32 mesh points based on Gauss-Hermite rule. When the residual is less than 1×10^{-6}, the calculation is considered to be convergent.

3.4.1 Influence of component concentration ratio on the molecular transport of engine internal and external mixed flow field

Consider an engine internal and external mixed flow for two-component gas mixture. Parameters are set as follows: mass ratio $m_2/m_1=0.5$, diameter ratio of component particles $d_2/d_1=1$ and inlet Knudsen number $Kn=0.0009$. Component concentration is set to three states. State 1: concentration of component 1 is 0.3 and concentration of component 2 is 0.7. State 2: concentration of component 1 is 0.5 and concentration of component 2 is 0.5. State 3: concentration of component 1 is 0.7 and concentration of component 2 is 0.3.

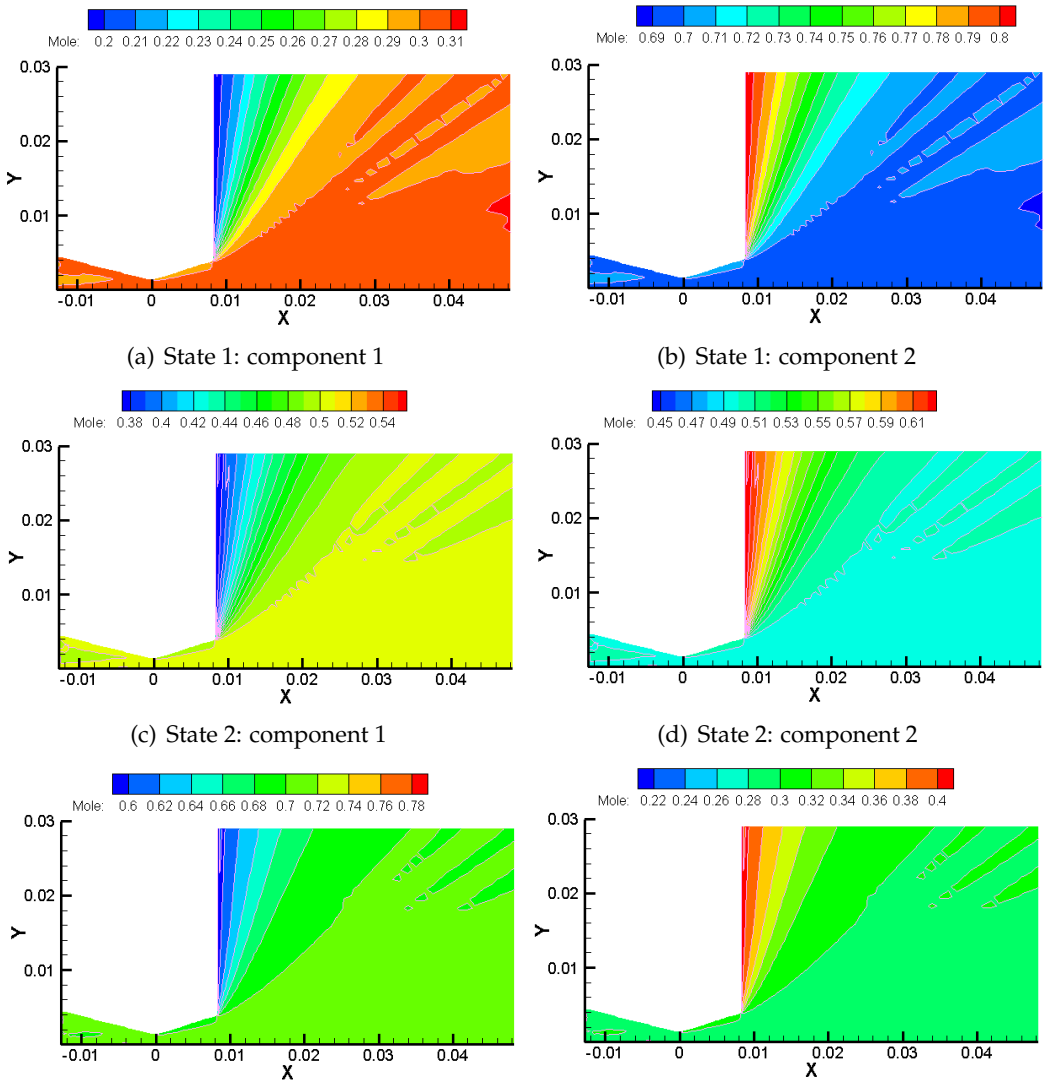

(a) State 1: component 1 (b) State 1: component 2

(c) State 2: component 1 (d) State 2: component 2

(e) State 3: component 1 (f) State 3: component 2

Figure 11: Mole fraction contour distributions of each component in the flow field under three concentration ratio states.

Fig. 11 shows the mole fraction contour distributions of each component in the flow field for the three concentration ratio states. It can be seen from the figure that there is a large diffusion phenomenon in each component of the flow field under the three different concentration ratios. Among them, the relatively heavy component 1 molecules are mainly distributed along the axis, while the light component 2 molecules are diffused around, especially in the backflow region, there are more component 2 molecules and there is a stratification phenomenon. There is concentration separation in external field,

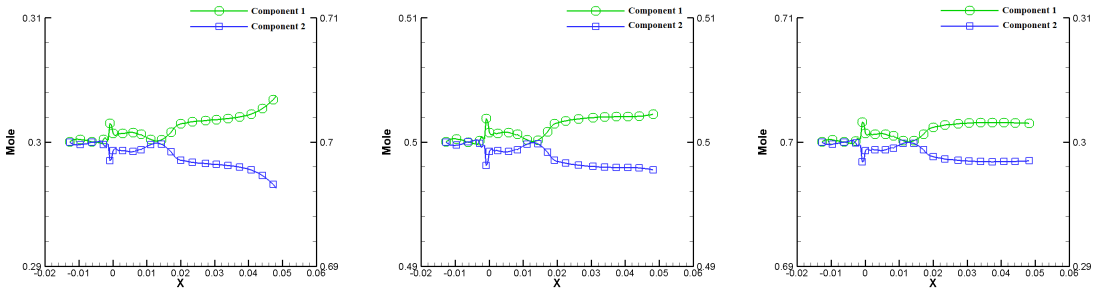

(a) State 1 (b) State 2 (c) State 3

Figure 12: Mole fraction distributions of each component along the flow field axis for three concentration ratio states.

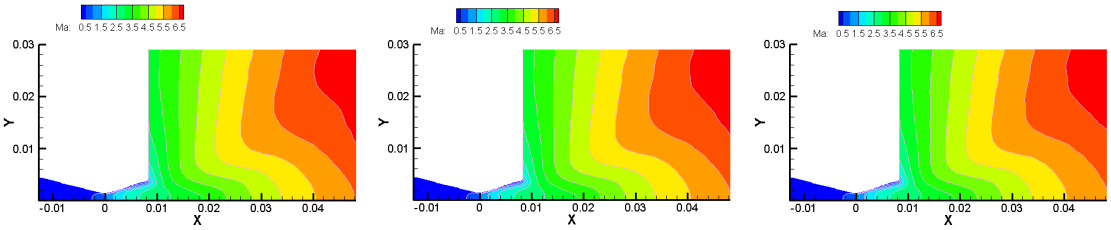

(a) State 1 (b) State 2 (c) State 3

Figure 13: Mach number contour distributions of gas mixture in the flow field for three concentration ratio states.

but the separation is not complete, and there is still a mixing region. As can be seen from Fig. 12, the mole fraction of component 1 distributed along the axis increases, but the increase is not large. When the concentration ratio between the molecules of component 2 and component 1 is gradually reduced, the mole fraction of the gas mixture under different states is basically the same, which shows that when $Kn=0.0009$, the concentration ratio has little influence on the diffusion of components.

Figs. 13 and 14 show the Mach number contour and axial distributions of gas mixture for the three concentration ratio states. As can be seen from Fig. 13, the distributions of Mach number contour of the flow field calculated under different component concentration ratios are basically consistent, indicating that when $Kn=0.0009$, changing the component concentration ratio has little influence on the macroscopic flow parameters of the flow field. The results in Fig. 14 also confirm the above conclusion. As can be seen from Fig. 14, the Mach number distribution curves at the axis of the three states basically coincide, and there is only a slight difference at the end of the external field axis, indicating that when $Kn=0.0009$, Mach number of gas mixture is not affected by the concentration ratio of components.

Fig. 15 shows the axial velocity distributions of gas mixture along the axis for the

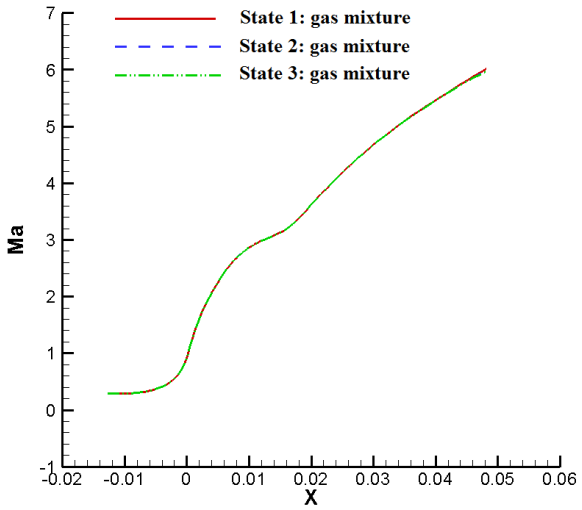

Figure 14: Mach number distributions of gas mixture along the axis under three concentration ratio states.

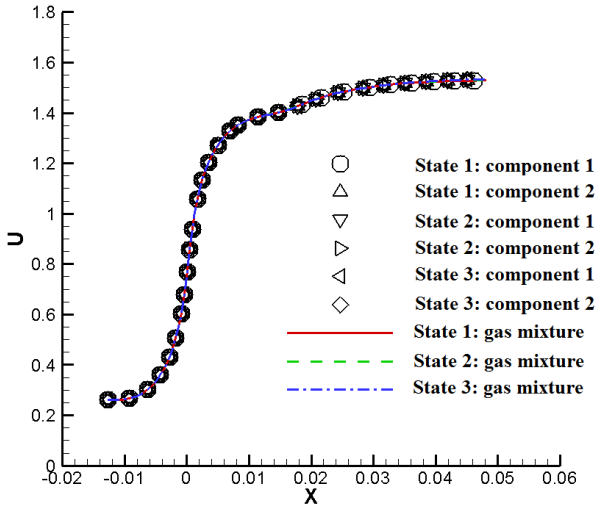

Figure 15: Axial velocity distributions of gas mixture along the axis under three concentration ratio states.

three concentration ratio states. It can be seen from the figure that the axial velocity of components is basically consistent under different concentration ratios, indicating that when $Kn=0.0009$, the component concentration ratio has little effect on the axial velocity of each component, and there is almost no difference in the axial velocity between the

components. Under different concentration ratios, the axial velocity of gas mixture is basically the same, indicating that when $Kn=0.0009$, the component concentration ratio has almost no effect on the axial velocity of gas mixture. Under different concentration ratios, the axial velocity of components is basically consistent with the axial velocity of gas mixture, indicating that when $Kn=0.0009$, the influence of component concentration ratio on the collision frequency between the components is small, and the collision between the components is frequent, and there is sufficient momentum and energy exchange.

3.4.2 Influence of component mass ratio on molecular transport of engine internal and external mixed flow field

Consider an engine internal and external mixed flow for multi-component gas mixture. Parameters are set as follows: concentration of component 1 is 0.5, concentration of component 2 is 0.5, diameter ratio of component particle d_2/d_1=1, and inlet Knudsen number is $Kn=0.0009$. Component mass ratio m_2/m_1 is set to three states. State 1: $m_2/m_1=0.5$. State 2: $m_2/m_1=0.25$. State 3: $m_2/m_1=0.2$.

Figs. 16 and 17 show the mole fraction contour and axis distributions of each component in the flow field for the three mass ratio states. It can be seen from Fig. 16 that the diffusion law of each component in the flow field under three different mass ratios is similar to that in Fig. 11: heavy component diffuses along the axis and light component diffuses to backflow region, and the mole fraction of light component in the backflow region increases with the decrease of mass ratio. Fig. 17 confirms the above law, the mole fraction of component 1 distributed along the axis increases, and the mole fraction of component 2 decreases. By comparing (a), (b) and (c) in Fig. 17, it can be seen that as the mass ratio of component 2 to component 1 decreases, the mass difference between two components increases, and the variation degree of the mole fraction of component 1 along the axis increases, indicating that as the mass ratio between heavy component and light component increases, the component diffusion degree increases and the diffusion phenomenon becomes more obvious.

Figs. 18 and 19 show the Mach number contour and axis distributions of gas mixture for three mass ratio states. It can be seen from Fig. 18 that the distributions of Mach number contour calculated in the flow field are different under different mass ratios of components, indicating that when $Kn=0.0009$, changing the mass ratio of components has a certain impact on the macroscopic flow parameters of the flow field. The results in Fig. 19 also confirm the above conclusions. It can be seen from Fig. 19 that the Mach number distribution curves at the axis of three states basically coincide, and there is a slight difference at the end of the external field axis. The reason is that when $Kn=0.0009$, momentum and energy are fully exchanged between the components, so the Mach number axis distribution curves basically coincide. The Mach number distribution of gas mixture is not strictly consistent, and there is a phenomenon that the Mach number of state 3 is the highest, state 2 is the second, and state 1 is the lowest. Comparing Figs. 14 and 19, we can see that mass ratio has a greater influence on the Mach number of gas mixture than concentration ratio.

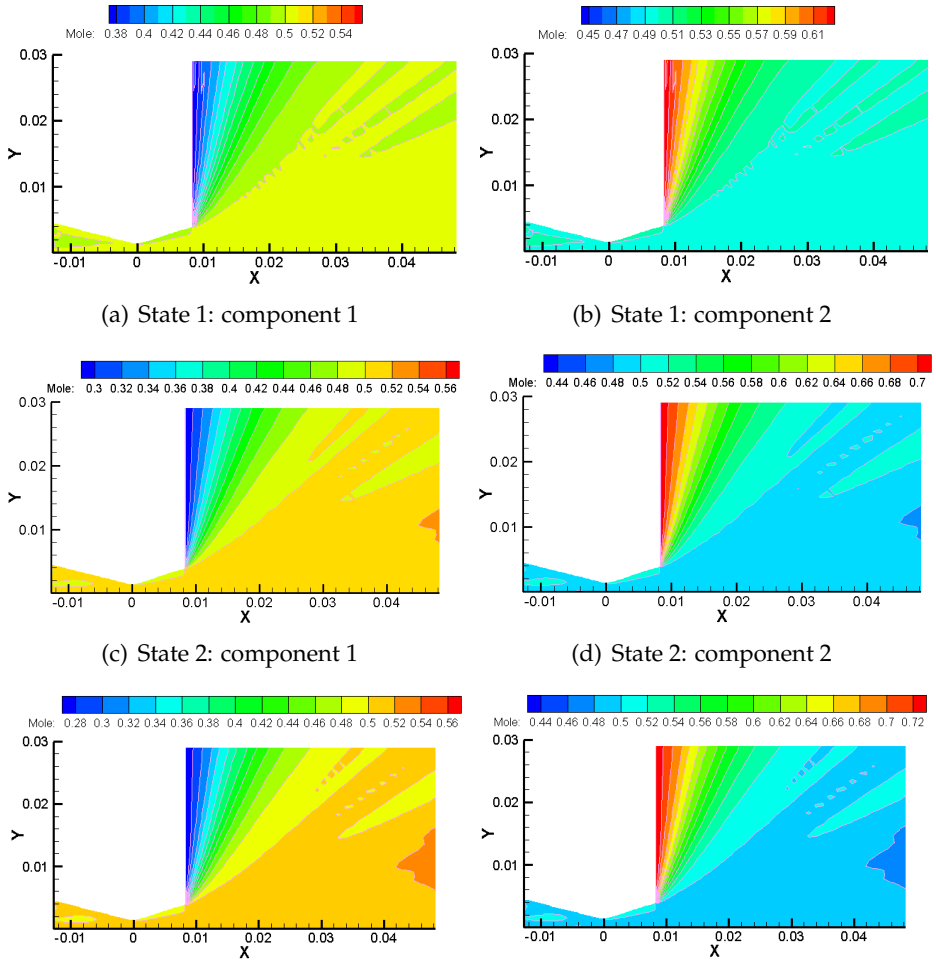

(a) State 1: component 1 (b) State 1: component 2

(c) State 2: component 1 (d) State 2: component 2

(e) State 3: component 1 (f) State 3: component 2

Figure 16: Mole fraction contour distributions of each component in the flow field under three mass ratio states.

Fig. 20 shows the axial velocity distributions of gas mixture along the axis for three mass ratio states. It can be seen from the figure that the axial velocities between components, between gas mixtures, and between components and gas mixture are very close, and the essential reason is that $Kn=0.0009$, and the collision frequency between particles of components is high. By comparing Fig. 15 and Fig. 20, it can be found that although the axial velocities of gas mixture under different concentration ratios and different mass ratios are very close, the differences between gas mixture under different mass ratios are significantly different from those under different concentration ratios, which again indicates that the influence of mass ratio is greater than that of concentration ratio. As for how much the mass ratio affects the axial velocity of gas mixture, this needs to be an-

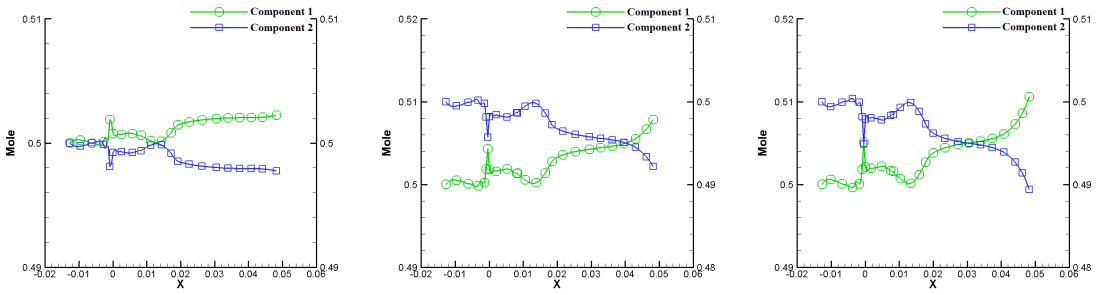

(a) State 1 (b) State 2 (c) State 3

Figure 17: Mole fraction distributions of each component along the flow field axis for three mass ratio states.

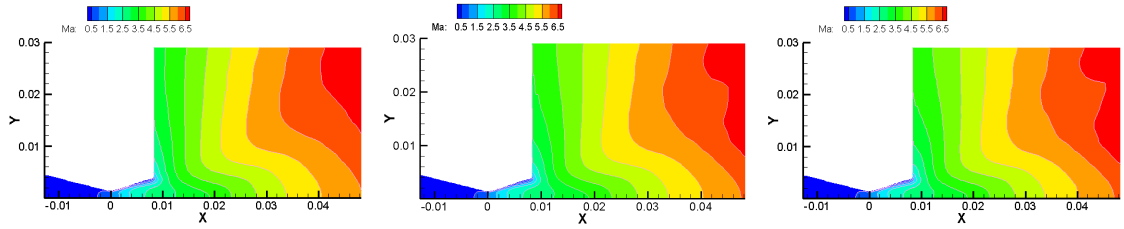

(a) State 1 (b) State 2 (c) State 3

Figure 18: Mach number contour distributions of gas mixture in the flow field for three mass ratio states.

alyzed in combination with the effects of different rarefaction states on the components and gas mixture.

4 Conclusion

In this paper, gas-kinetic unified algorithm is extended to multi-component monatomic gas mixture flow. In order to verify the existing scheme, the steady normal shock wave structure problem, the flow around two-dimensional circular cylinder and the pressure/temperature driven microchannel flow problems under different mass ratios are simulated. The simulation results are in good agreement with the existing results, which verifies the reliability of the algorithm. Then, 25N attitude control engine two-dimensional profile nozzle internal and external mixed flow problem is studied, and the influences of component concentration ratio and mass ratio on molecular transport in the engine internal and external mixed flow field are explored. The results show that the component concentration ratio has little effect on the molecular transport in the mixed flow field when Knudsen number is small. As the mass ratio between heavy component and light component increases, the degree of component diffusion increases, and the dif-

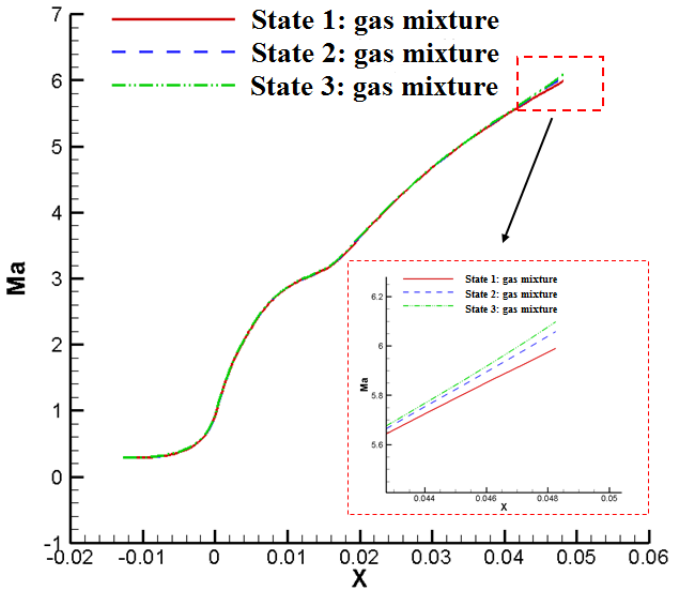

Figure 19: Mach number distributions of gas mixture along the axis for three mass ratio states.

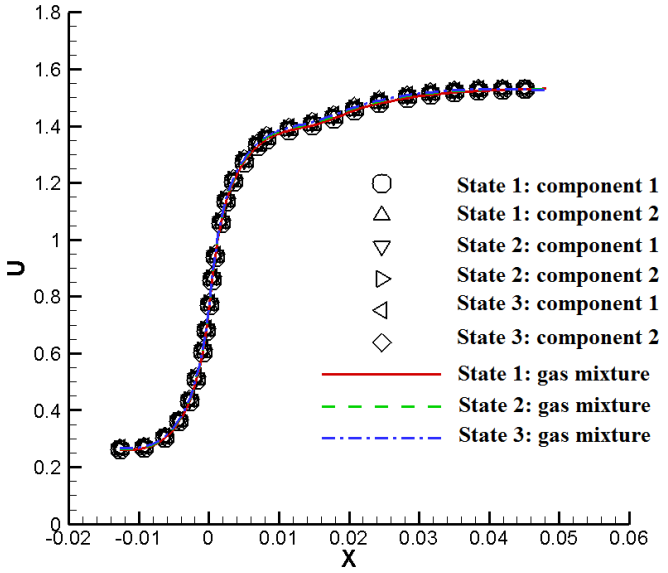

Figure 20: Axial velocity distributions of gas mixture along the axis for three mass ratio states.

fusion phenomenon becomes more obvious. The effect of component mass ratio on gas mixture flow parameters is greater than that of concentration ratio.

Acknowledgments

This work is supported by the National Natural Science Foundation of China (12332013). The authors are thankful to the editors and reviewers for their valuable comments and suggestions, which greatly improved the quality of the manuscript.

References

[1] F. Sharipov and D. Kalempa, Gaseous mixture flow through a long tube at arbitrary Knudsen numbers, Journal of Vacuum Science and Technology A: Vacuum, Surfaces, and Films, 20 (2002), 814-822.
[2] S. Takata and K. Aoki, The ghost effect in the continuum limit for a vapor-gas mixture around condensed phases: Asymptotic analysis of the Boltzmann equation, Transport Theory and Statistical Physics, 30 (2001), 205-237.
[3] S. Naris, D. Valougeorgis, D. Kalempa and F. Sharipov, Flow of gaseous mixtures through rectangular microchannels driven by pressure, temperature, and concentration gradients, Physics of Fluids, 17 (2005), 100607.
[4] F. Sharipov, Gaseous mixtures in vacuum systems and microfluidics, Journal of Vacuum Science and Technology A, 31 (2013), 050806.
[5] Z. H. Li, Z. H. Li, J. L. Wu and A. P. Peng, Coupled Navier–Stokes/direct simulation Monte Carlo simulation of multicomponent mixture plume flows, Journal of Propulsion and Power, 30 (2014), 672-689.
[6] J. M. Burt and I. D. Boyd, A hybrid particle approach for continuum and rarefied flow simulation, Journal of Computational Physics, 228 (2009), 460-475.
[7] R. Wang and K. Xu, Unified gas-kinetic scheme for multi-species non-equilibrium flow. In: Proceedings of AIP Conference Proceedings, (2014), 970-975.
[8] Y. Zhang, L. H. Zhu, R. J. Wang and Z. L. Guo, Discrete unified gas kinetic scheme for all Knudsen number flows. III. Binary gas mixtures of Maxwell molecules, Physical Review E, 97 (2018), 053306.
[9] Y. Zhang, L. H. Zhu, P. Wang and Z. L. Guo, Discrete unified gas kinetic scheme for flows of binary gas mixture based on the McCormack model, Physics of Fluids, 31 (2019), 017101.
[10] J. L. Wu, Z. H. Li, A. P. Peng, X. C. Pi and X. Y. Jiang, Utility computable modeling of a Boltzmann model equation for bimolecular chemical reactions and numerical application, Physics of Fluids, 34 (2022), 046111.
[11] F. Fei, J. Zhang, J. Li and Z. H. Liu, A unified stochastic particle Bhatnagar-Gross-Krook method for multiscale gas flows, Journal of Computational Physics, 400 (2020), 108972.
[12] Y. J. Zhu, C. Liu, C. W. Zhong and K. Xu, Unified gas-kinetic wave-particle methods.II.Multiscale simulation on unstructured mesh, Physics of Fluids, 31 (2019), 067105.
[13] C. Liu and K. Xu, A unified gas kinetic scheme for continuum and rarefied flows V: multiscale and multi-component plasma transport, Communications in Computational Physics, 22 (2017), 1175-1223.
[14] T. Xiao, K. Xu and Q. Cai, A unified gas-kinetic scheme for multiscale and multicomponent flow transport, Applied Mathematics and Mechanics, 40 (2019), 355-372.
[15] C. Lin, K. H. Luo, A. Xu, Y. Gan and H. Lai, Multiple-relaxation-time discrete Boltzmann modeling of multicomponent mixture with nonequilibrium effects, Physical Review E, 103 (2021), 013305.

[16] P. Andries, K. Aoki and B. Perthame, A consistent BGK-type model for gas mixtures, Journal of Statistical Physics, 106 (2002), 993-1018.
[17] F. J. McCormack, Construction of linearized kinetic models for gaseous mixtures and molecular gases, Physics of Fluids, 16 (1973), 2095-2105.
[18] Z. H. Li and H. X. Zhang, Gas-kinetic numerical studies of three-dimensional complex flows on spacecraft re-entry, Journal of Computational Physics, 228 (2009), 1116-1138.
[19] Z. H. Li, A. P. Peng, H. X. Zhang and J. Y. Yang, Rarefied gas flow simulations using high-order gas-kinetic unified algorithms for Boltzmann model equations, Progress in Aerospace Sciences, 74 (2015), 81-113.
[20] Z. H. Li and H. X. Zhang, Numerical investigation from rarefied flow to continuum by solving the Boltzmann model equation, International Journal for Numerical Methods in Fluids, 42 (2003), 361-382.
[21] F. Li, Z. H. Li and A. G. Chen, Boltzmann-Rykov model equation gas-kinetic unified algorithm and nozzle flow, Journal of Beijing University of Aeronautics and Astronautics, 1-17.doi:10.13700/j.bh.1001-5965.2023.0054.
[22] A. P. Peng, Z. H. Li, J. L. Wu and X. Y. Jiang, Validation and analysis of gas-kinetic unified algorithm for solving Boltzmann model equation with vibrational energy excitation, Acta Physica Sinica, 66 (2017), 204703.
[23] J. L. Wu, Z. H. Li, Z. B. Zhang and A. P. Peng, On derivation and verification of a kinetic model for quantum vibrational energy of polyatomic gases in the gas-kinetic unified algorithm, Journal of Computational Physics, 435 (2021), 109938.
[24] J. L. Wu, Z. H. Li, A. P. Peng, X. C. Pi and X. Y. Jiang, Utility computable modeling of a Boltzmann model equation for bimolecular chemical reactions and numerical application, Physics of Fluids, 34 (2022), 046111.
[25] Z. H. Li, J. L. Wu, X. Y. Jiang and Q. Ma, A massively parallel algorithm for hypersonic covering various flow regimes to solve Boltzmann model equation, Acta Aeronautica et Astronautica Sinica, 36 (2015), 201-212.
[26] F. Li, Z. H. Li, X. Y. Jiang, W. Q. Hu, Z. H. Li and W. Q. Luo, Gas-kinetic unified algorithm for two-dimensional planar and axisymmetric nozzle flows, International Journal for Numerical Methods in Fluids, 95 (2023), 1617-1638.
[27] Z. H. Li, W. Q. Hu, A. P. Peng, J. L. Wu and C. H. Lee, Gas-kinetic unified algorithm for plane external force-driven flows covering all flow regimes by modeling of Boltzmann equation, International Journal for Numerical Methods in Fluids, 92 (2020), 922-949.
[28] Z. H. Li, A. P. Peng, Q. Ma, L. N. Dang, X. W. Tang and X. Z. Sun, Gas-kinetic unified algorithm for computable modeling of Boltzmann equation and application to aerothermodynamics for falling disintegration of uncontrolled Tiangong-No. 1 spacecraft, Advances in Aerodynamics, 1 (2019), 1-21.
[29] H. X. Zhang and F. G. Zhuang, NND Schemes and Their Applications to Numerical Simulation of Two- and Three-Dimensional Flows, Advances in Applied Mechanics, 29 (1991), 193-256.
[30] G. A. Bird, Molecular Gas Dynamics and the Direct Simulation of Gas Flows, Oxford: Claredon Press, (1994).
[31] G. A. Bird, The DS2V/3V Program Suite for DSMC Calculations, 24th International Symposium on Rarefied Gas Dynamics, (2005), 541-546.
[32] S. Kosuge and S. Takata, Database for flows of binary gas mixtures through a plane microchannel, European Journal of Mechanics - B/Fluids, 27 (2008), 444-465.
[33] C. Cercignani, The Boltzmann Equation and its Applications, Springer-Verlag, 1988.